Silicon (2019) 11:1925–1937
https://doi.org/10.1007/s12633-018-0008-9

ORIGINAL PAPER

Study of Infra-red Spectroscopy on Bonding Environment and Structural Properties of Nanocrystalline Silicon Thin Films Grown by VHF-PECVD Process

Sucheta Juneja[1,2,3] · **Mansi Sharma**[1,2] · **Sushil Kumar**[1,2]

Received: 16 May 2018 / Accepted: 2 November 2018 / Published online: 16 November 2018

Abstract

Infra-red spectroscopy as an effective tool used to establish platelet like configuration in nanocrystalline silicon thin films (nc-Si:H). These films were deposited using 60 MHz assisted very high frequency plasma enhanced chemical vapor deposition process with varying pressure from 4 to 40 Pa. The deposited films were characterized by X-ray diffraction (XRD), Field emission scanning electron microscopy (FESEM), Atomic force microscopy (AFM), Raman spectroscopy (RS), Fourier transform infra-red spectroscopy (FTIR), Dark conductivity, UV-Vis Spectra and photosensitivity. Infra-red studies of these films reveals that the hydrogen bonding is a platelet like configuration (Si-H groups at 2033 cm^{-1}) located at grain boundaries resulting in crystalline grains wrapped with hydrogen rich amorphous tissues that provides good passivation resulting in less dangling bonds on grain boundary surface. Structural transformation from amorphous silicon (a-Si:H) to nanocrystalline (nc-Si:H) phase has been identified at pressure of 24 Pa. The increase in deposition pressure provides clear evidence of improved crystallinity (∼ 37%) which were depicted by increased grain size (∼ 12 nm), reduced hydrogen bonded content (∼ 5.0%), widening of optical gap (∼ 1.9 eV) with enhanced polymerization in the network.

Keywords Thin films · Vapor deposition · Nano-crystalline materials · Raman spectroscopy · X-ray diffraction · Microstructure

1 Introduction

Hydrogenated amorphous silicon has gained much interest due to its optical, electrical properties and low-cost device applications i.e. silicon thin film based solar cells, thin film transistors etc. [1]. However, the material suffers from serious drawback i.e. Light- induced degradation, or called Staebler -Wronski effect [2] and it restricts in making stable devices. Intrinsic nanocrystalline material has the potential to completely overcome the drawback of amorphous silicon and received extensive scientific and technological interest as a solar cell material in recent years due to possessing superior important properties such as higher electrical conductivity, higher carrier mobility, higher doping efficiency, superior stability and band gap tailoring [3–7]. Nanocrystalline material also referred to as diphasic material consists of nanometer sized grains embedded in an amorphous matrix [8]. Diphasic silicon films (a-Si:H/nc-Si:H) have been deposited in a new regime of plasma enhanced chemical vapor deposition in the region closest of phase transition from amorphous to crystalline state. This is defined as transition region in the deposited films. Nanocrystalline silicon fascinates when combined with amorphous silicon in tandem configuration (commonly known as "nanomorph") solar cells due to difference in optical band gaps of these materials allowing conversion of large part of solar spectrum. In such structures, top a-Si:H cell absorbs wavelength of light upto visible region

✉ Sushil Kumar
skumar@nplindia.org

[1] CSIR – National Physical Laboratory, Dr. K.S. Krishnan Marg, New Delhi, 110012, India

[2] Academy of Scientific and Innovative Research (AcSIR), CSIR-NPL Campus, Dr. K.S. Krishnan Marg, New Delhi, 110012, India

[3] Indian Institute of Technology, Delhi (IITD), Hauz Khas, New Delhi, 110016, India

and bottom μc/nc-Si:H cell can absorbs light in near infrared region enhances the spectral response, allowing for larger attainable conversion efficiencies [9, 10]. The properties of nanocrystalline silicon thin films are mainly associated with the bonding configuration of hydrogen and hydrogen content in the structure [11, 12]. It might be considered that hydrogen bonding configurations is a consequence of structure. Therefore, it is necessary to investigate the hydrogen bonding and their interaction with different bonding sites in the structure and it has been widely investigated. This understanding results in material with good opto-electronic properties.

Nanocrystalline silicon thin films deposited by Plasma Enhanced Chemical Vapor Deposition (PECVD) process has gained significant attention due to its better stability under light compared to amorphous silicon for solar cell applications [13, 14]. However, control of crystallinity is crucial in these films as it influence considerably the material properties [15]. Among various PECVD process parameters, the deposition pressure largely influences the structural properties of these materials and is primarily responsible for secondary gas phase reaction during growth of films [16, 17]. At higher pressure discharge, less mean free path of species /ions which increases the gas residence time in the deposition chamber. The difficulty arises at high pressure discharge under high hydrogen dilution are powder formation, non- stability of plasma that might be reduced by optimizing the deposition conditions. At higher pressures, the concentration of hydrogen in the plasma are recognized to etch preferentially amorphous tissue and the heat (exothermic) generated during etching allows local re-crystallization by chemical annealing [18, 19]. Conventionally, radio frequency (RF) excitation frequency (13.56 MHz) is used for plasma discharge of silane diluted in hydrogen for the development of silicon films containing crystallites. Alternatively, it is concluded that higher excitation frequencies are found to be more compatible for formation of crystalline phase with higher deposition rate [20]. The higher frequency results in increased electron density with decreases the electron temperatures and plasma potential because of wave-riding effect [21].

It is possible to produce highly dense plasma with optimized deposition conditions for the growth of amorphous and nanocrystalline films with high deposition rate without deteriorate the surface of film. The main aim of present investigation is to study the effect of pressure on hydrogen bonding with related structural, optical and electrical properties of silicon thin films deposited using 60 MHz assisted PECVD process. The deposited films were analyzed using structural, optical and electrical characterization techniques. The present work insights the effect of very high frequency pressure conditions on silicon films keeping all other parameters constant.

2 Experimental

The amorphous and nc-Si: H thin films were deposited in capacitive-coupled parallel plate VHF PECVD system. Corning glass # 7059, transparent conducting oxide (TCO) glass and silicon wafers are used as substrates for deposition and the deposition parameters are shown in Table 1. The precursor gas was ultra-high purity silane mixture (5% SiH_4 diluted in hydrogen). The deposition pressure was varied from 4 to 40 Pa keeping substrate temperatures (270°C) and power density (90 mW/cm^2) fixed. The thickness of films was in the range of 50 to 80 nm measured by a Stylus profilometer (Nanomap 500 ES). The optical properties of samples were measured using a double monochromator (Shimadzu UV-2450 spectrophotometer). The crystallinity and mean crystallite size in the deposited films was estimated using Raman spectroscopy (via LabRAM HR800, Horiba JY spectrometer) and X-ray diffraction (XRD via Rigaku) studies. In Raman spectroscopy, excitation of the samples was performed by air cooled He-Ne laser tuned at 632 nm (Spectra Physics). Measurements were recorded at room temperature in the back scattering geometry on glass substrates using a 50 X LWD microscope objective with NA = 0.75. The laser was fixed at nearly 1 μm spot size also the power density was kept low to avoid laser induced crystallization or excessive heating on probe region. X-ray measurements were carried using conventional (Cukα) X-ray radiation (λ = 1.54Å). XRD measurements were also carried on glass substrate. The average crystallite size were estimated from full width at half maxima (FWHM) of <111> peak using Scherrer formula. Different silicon and hydrogen bonding configuration and bonded hydrogen content (C_H) were analyzed using Fourier transform infra red spectroscopy (FTIR) on silicon wafer substrates. In order to avoid the effect of signals from the substrate the corresponding reference spectra for substrate observed during characterization were subtracted from the sample spectra. Microstructure parameter (R*) has been calculated by stretching mode vibrational spectra of Si:H films. Field emission scanning electron microscopy (FESEM)

Table 1 Deposition parameters for amorphous and μc/nc-Si: H films deposited by VHF-PECVD

Deposition parameters	
Base vacuum	: 4×10^{-6}Pa
Substrate temperature	: 270°C
Power density	: 90 mW/cm^2
Pressure variation	: 4–40 Pa
SiH_4 Flow rate	:47 sccm
Deposition time	: 10 min

images were acquired from FEI Nova NanoSEM 450 electron microscope. Atomic force microscopy (AFM) was performed to investigate surface morphology and roughness in the deposited films using Veeco Digital Instruments Nanoscope V.

3 Results and Discussion

3.1 UV-VIS Spectroscopy

The absorbance spectra and absorption spectrum versus energy (hυ) in silicon films deposited at varying pressures is shown in Fig. 1a, b respectively. The optical band gap (E_g) has been calculated from absorption measurements using the Tauc's equation by extending the tangent to the curve on x-axis, the intercept of which gives the value of material band gap [22]

$$(\alpha h\upsilon)^{1/2} = B\left(h\upsilon - E_g\right) \quad (1)$$

Where hυ is the energy of light, E_g is optical band gap, B is the constant known as the edge-width parameter which is related to disorderness in the material in terms of bond length or bond angle and α is absorption coefficient [23]. The (α) can be calculated with the formulae; $\alpha = \frac{1}{d}\ln\left(\frac{1}{T} - R\right)$ [24]; where d named as thickness of film, T is transmission and R is reflection spectra using UV-spectrophotometer. In the present investigation, the band gap value rises from 1.75 to 1.94 eV as pressure varies from 4 to 30 Pa then decreases to 1.71 eV with further increase of pressure to 40 Pa. The band gap of 1.94 and 1.89 eV exhibited by a film deposited at a pressure of 24 and 30 Pa respectively. These films also showed higher crystallinity and conductivity values. The higher energy band gap around 2 eV in these films was associated with nc-Si:H. The band gap of nc-Si:H films is higher than those of a-Si:H (i.e.1.7 to 1.8 eV) [25]. The change in band gap depends on the form and content of hydrogen bonding in the silicon films [26]. It is already reported that band gap value increases with increase of nanoclusters of nc-Si:H in a-Si:H matrix [27]. Vasiliev et al. [28] used time–dependent local density approximation (TDLDA) to show the increase of band gap with decrease of cluster size in the silicon nanostructures. There still exists several ambuiguities related with band gap of nc-Si:H thin films hence entire microscopic perceptive of band gap is still lacking. Nevertheless, one of the established models for nanometric materials is quantum confinement [29]. According to a quantum confinement mode, the optical band gap depends on the size of nc-Si:H. The different absorption properties are explained by a combination of the heterogeneous microstructure of the films (amorphous and nanocrystalline) characterized by crystalline volume fraction and quantum confinement effects in the nanocrystallites which depends on the crystallite size and its distribution. In the present case, films deposited at pressures 24 Pa and 30 Pa produces more atomic hydrogen during deposition. It is already reported that higher dilution favors nanocrystalline growth. In case of nanocrystalline growth the presence of atomic hydrogen provides more nucleation sites on the growing surface thus helps in reconstructing silicon structure favouring strong silicon –silicon (Si-Si) bonds with breaking of weak/strained silicon-hydrogen (Si-H) bonds in the network. Therefore, in nanocrystalline silicon bonded hydrogen content (i.e. Si-H) reduces. This results in increased size of nanocrystallites with increase in density of crystalline regions during deposition. It can even improve the agglomeration of adjacent nanocrystallites during

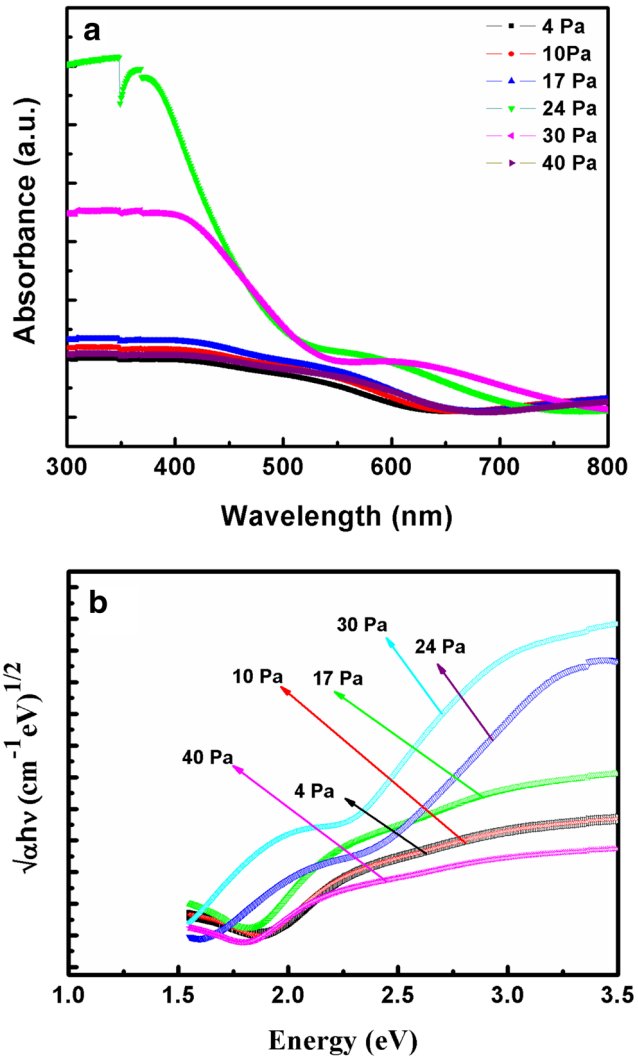

Fig. 1 **a** Absorbance plot of silicon films deposited at various pressure (Pa); **b** Tauc plot of silicon films deposited at various pressure (Pa)

growth. Consequently, bigger sized crystals are formed which eventually decreases the intensity of absorption coefficient in visible and infrared region.

3.2 Infra Red Absorption Study

To investigate silicon monohydride configuration and hydrogen content, Fourier transform infrared spectroscopy has been used. The FTIR spectra of films deposited at varying pressures was shown in Fig. 2. Figure 2 showed the different Si-H of absorption peak that can be observed at ~630, 880 and 2090 cm^{-1} respectively in the infrared spectra of deposited films and are named accordingly as wagging/rocking mode, bending mode and stretching mode [30, 31]. The peak obtained at 1000 cm^{-1} is associated with Si-O stretching mode which indicates undesired incorporation of oxygen in samples. The large concentration of oxygen was asssumed to be associated with the origination of Si-O/ Si interface dangling bond defects [32, 33]. The main absorption band for SiO_2 connected with stretching vibrations of bridging oxygen atoms is known to be within the wave number range 1000–1100 cm^{-1}, and the position of the peak determined by the structural arrangement of the oxygen atoms [34]. The source of this oxygen is simply post oxidation. The deposited films on air exposure become oxidized. The oxidation after air exposure depends on the structures of the deposited films. Oxygen principally is an electronically active impurity that significantly worsens the transport properties of the films, so its diffusion into the bulk material should be minimized. Regarding measurements under illumination, incident photons seemed to be accountable for the breaking of strained/weak bonds which ultimately led to

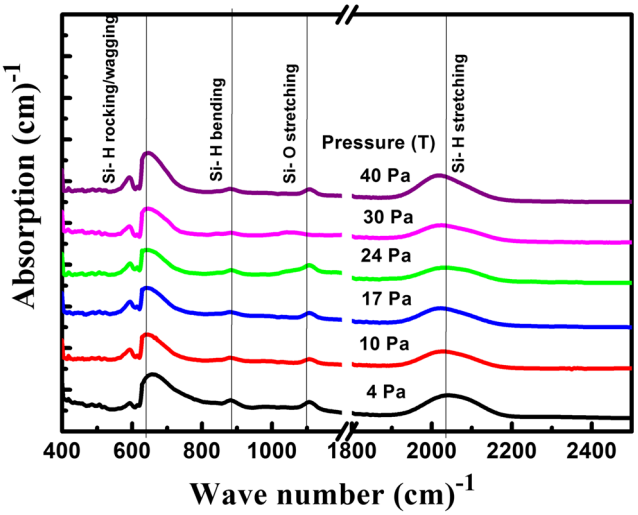

Fig. 2 Infra-red absorption spectra of silicon thin films deposited at different pressures as indicated

the incorporation of oxygen atoms into the structure [35]. The bonded hydrogen content (C_H) of silicon films has been estimated from the integrated intensity of absorption peak nearly at ~630 cm^{-1} using the following formulae [36, 37]

$$C_H = \frac{Aw}{NSi} \int \frac{\alpha(\upsilon)}{\upsilon} \tag{2}$$

Where α (υ) termed as the absorption coefficient of the film, (υ) as wave number in cm^{-1} and oscillator strength $A_w = 2.1 \times 10^{19} cm^{-2}$, $N_{si} = 5 \times 10^{22}$ cm^{-3} named as the atomic density [38]. Table 2. Showed the calculated hydrogen content of all the deposited films. The hydrogen content was found to be in the range 5-14%.

Figure 3a represents the decomposition of Infra-red absorption spectra of Si-H stretch for film deposited at 30 Pa pressure. Five hydride modes are identified related to distinct bonding configurations. The stretching mode of hydride relies on few factors, for example, such as local density of hydrides, and all the conceivable shared dipole interactions of hydrogen incorporation configurations [39]. Bonding of hydrogen in amorphous silicon takes either in the form of clusters or the random distribution of hydrogen in the network sites [40, 41]. The hydrogen clusters arise due to internal surfaces of microvoids or, named as hydrogen platelets configurations. These hydrogen platelets configurations are similar to c-Si along <111> plane [42, 43]. It is known that the clustering taking place on internal voids leads to poor electronic property in a-Si:H, while clustering inside the platelets results in superior quality material compared to c-Si [44]. The five hydride modes are named as low stretching mode (LSM), in the range 1980-2010 cm^{-1} related to isolated monohydrides formed by dispersion of dangling bonds and are profound states in hydrogen density of states (HDOS). High stretching mode (HSM), lie in 2070 - 2100 cm^{-1} range originate from amorphous tissue in nanocrystalline film, where both di-hydrides and clustered monohydrides are lying on the surface of voids which are also shallow states in HDOS. The extreme HSM lies in the range 2140 - 2150 cm^{-1} and are associate with the

Table 2 Shows Bonded Hydrogen content & microstructure parameter in silicon films deposited at different pressure

Pressure (Pa)	Bonded hydrogen content (C_H) (%)	Microstructure parameter (R*)
4	7.4	0.42
10	8.6	0.37
17	10.7	0.34
24	6.7	0.30
30	5.3	0.28
40	14.2	0.31

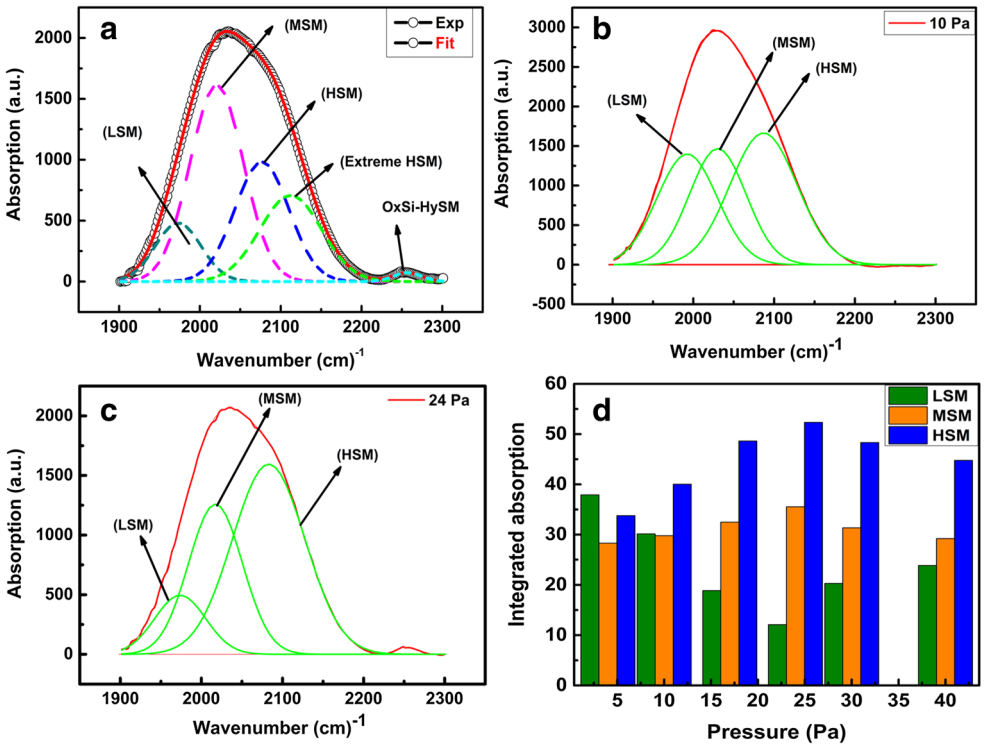

Fig. 3 **a** Decomposition of FTIR spectra of the Si-H stretching mode for film deposited at 30 Pa. The solid curve represents the total fit and dashed curve represents the Gaussian shaped five different stretching modes; **b** Decomposition of stretching modes into LSM, MSM and HSM of a typical silicon film deposited at 10 Pa; **c** Decomposition of Si:H stretching modes for film deposited at 24Pa. **d** Integrated absorption of LSM, MSM and HSM of Silicon thin films deposited at different process pressures

trihydrides configuration in the film. Mainly the middle or center stretching mode (MSM) lies almost at ~2033 cm^{-1} attributable to clusters of Si-H groups in platelet like configurations, grown by incorporation of hydrogen into the weak/frail Si-Si bonds that are shallow states like hydride vibrations located at platelet resembling configurations at amorphous – crystalline edges or at the grain borders [45–47]. The stretching mode appears at ~2250 cm^{-1} relates to $O_mSi\text{-}H_n$ vibrations where the oxygen atoms are attached with atoms of silicon in back-holding arrangement, and thus collectively with 1000-1200 cm^{-1} reflects the bulk oxidation in film [48]. The presence of broad shoulder peak at ~2090 cm^{-1} has been observed for all the samples as shown in Fig. 2. This peak appears at ~2090 cm^{-1} can be attributed to the development of nano-sized crystallite silicon dispersed in an amorphous silicon material [49]. At pressure 24 and 30 Pa, the isolated hydrides may change to platelet like hydride groups indicated from stretching mode at ~2000 cm^{-1} shifts to higher wave number at ~2030 cm^{-1}, this attributes to hydride vibrations at the amorphous-crystalline interfaces resulting change in the microstructure i.e. amorphous to micro/nanocrystalline transition. At this pressure, large amount of hydrogen changes from isolated monohydrides mode to platelet mode. These platelet configurations are responsible for microstructure evolution if the material bounded by platelets is structurally relaxed. This structural relaxation leads to microcrystallinity in the material. Figure 3b illustrates the absorption of different modes LSM, MSM and HSM for Si: H film deposited at 10 Pa, deduced from decomposition of stretching modes. Figure 3c illustrates same the decomposition of Si:H stretching modes for film deposited at 24 Pa. First we will discuss the role of (LSM) and (HSM) which shows the change in hydrogen bonding configuration in deposited films. It has been observed that film deposited at low pressure is basically amorphous in nature beside with the dispersion of ultra nano - sized crystallites in silicon matrix as correlated from (FESEM) morphological images. The presence of crystallite phase out of the grain boundary where the notable contribution of boundaries is named as ultra - nanocrystalline silicon. From Fig. 3d, it has been observed that with increase in deposition pressure from 4 – 24 Pa the integrated absorption in (LSM) decreases shows that monohydrides located in vacancies of amorphous tissue whereas increase in (HSM) observed due to reduced amorphous fraction in films. The (HSM) results due to high kinetic energy of hydrogen atoms and ions in film deposition. Thus, dangling bond on the surface of voids is passivated by diffusing hydrogen. The bending mode observed at ~880 cm^{-1} reflects more dihydrides formation; these dihydrides are responsible for Staebler-Wronski effect [50]. Now, we discuss the role of (MSM) and very few studies focussed on this mode so far [51]. In this mode, silicon hydrides are present in platelet like configuration. Such platelet configurations are analogous to the configuration as observed in c-Si where the Si-H bonds are prevalently arranged along <111> plane which further correlates with (XRD) studies. MSM largely

influence on microstructure as well as on other properties of film because in the formation of MSM hydrides, insertion and diffusion of hydrogen are essential processes. In this process, hydrogen initiated crystallization of a-Si:H direct the formation of either bond-focused/centered (BC) hydrogen arrangement; where hydrogen atom is available in between two silicon atoms or either might in individual (Si-H) silicon monohydrides configurations where the possibility might be the hydrogen atom is clung with silicon leaving a dangling bond on another subsequent to breaking of frail/stressed Si-Si bond. The formation of platelet-like configuration comes about where Si-H bonds are there along a planar deformity, which means the grain boundaries, are produced quickly after the passivation of dangling bonds as situation discussed above via H diffusion. This configuration is analogous with the structures observed in c-Si where the Si-H bonds are prevalently arranged along <111> plane planar deformity. Thus, MSM hydrides provide good passivation. These hydrides influence largely on microstructure and other properties. From results, at pressures 24 and 30 Pa, the stretching mode shifts to higher wave number i.e. (MSM). The increase in (MSM) in platelet like configuration is due to diffusion of hydrides along grain boundaries. The MSM hydrides on a basic level structures forms a H-rich amorphous tissue encompassed the nano-sized crystalline grains that results in dense grain boundaries with good passivation. Hence, penetration of oxygen into the grain boundaries during films conservation brings about the post-deposition oxidation of the grain boundary surface that can be proficiently avoided [48]. It can be proposed that the films of higher absorption of (MSM) are H- rich regions within grain boundaries that are advantageous in avoiding post-deposition oxidation [52]. Therefore, we have examined the part of (MSM) hydrides on nc-Si:H films.

Information related to microstructure parameter (R*) can also be estimated from FTIR spectra. The microstructure factor (R*) defined as measurement of voids present within the material that definitely affects on the hydrogen bonding and microstructure of the material. The microstructure parameter R* was estimated using relation

$$R^* = \frac{(I_{2090})}{(I_{2090} + I_{2000})} \tag{3}$$

Where I_{2000} is the integrated absorption intensity attributable to isolated Si-H monohydrides, I_{2090} is the integrated absorption because of dihydrides or clustered bonding. It is reported that stronger the symmetric stretch band, lesser is the microstructure parameter. Results shown that the solar cells with reasonable conversion efficiencies obtained even with intrinsic layers exhibiting R* lies between 0.2-0.3 [53]. The microstructure parameter (R*) was given in Table 2. It was found that at pressure 24 and 30 Pa we obtained (R*) 0.32 and 0.28 respectively which is found at the transition region. The decrease in microstructure parameter indicates the presence of fewer voids into the material.

3.3 Formation of Platelet Configuration or (MSM) Stretching Mode

The insertion of H in strained Si-Si bonds leads to hydrogen platelet-like regions and the continuous insertion of hydrogen results in hydrogen clustering in platelets. From results, it can be observed that at pressure 24 and 30 Pa there is increased role of hydrogen platelet configuration in the network leading to hydrogen clustering in the platelets. After saturation, these platelet results more in open voids in the material and the hydrogen platelet configuration becomes bonded to internal surfaces. Therefore, IR absorption at nearly 2030 cm^{-1} shift to $\sim$2080 cm^{-1} for surface monohydride observed at pressure 40 Pa. This is due to the reason that after a certain absorption, the structure not support these hydrogen platelets and result in formation of internal voids and finally the etch rate increases due to weakening the network structure. This platelet configuration in the structure may be responsible for the evolution of crystallinity in the material. Hydrogen chemical potential is another important parameter determining the network disorder and the related transition towards crystalline growth in a-Si:H [54].

3.4 Raman Spectroscopy

Raman spectroscopy is a sensitive as well as direct tool to evidence the structural properties quantitatively of amorphous and crystalline component in the silicon thin films. Figure 4 shows the Raman spectra of silicon films deposited at varying deposition pressures. In literature, the broad shoulder peak distribution around 470-480 cm^{-1}, corresponds to TO mode of amorphous phase. The TO mode observed at nearly 490-500 cm^{-1} on the broad amorphous spectrum defined as intermediate component or grain boundary phase. There are different interpretations in literature regarding this intermediate or grain boundary component [55]. The peak position around 500 to 518 cm^{-1} can be interpreted as TO scattering form of different types of silicon grains. The TO vibrational mode or characteristic Raman peak of crystalline silicon results a sharp peak at 520 cm^{-1}. The Raman spectra of TO peaks can be best decomposed into three components using Gaussian line fitting method as shown in Fig. 5, the peak centred at $\sim$480 cm^{-1} representing the TO mode of amorphous silicon. From Fig. 4, at low pressure <24 Pa the peak position at 490 cm^{-1} can be observed. The peak centred at 490 cm^{-1} is due to contribution of small size crystallites (ultrananocrystals) [56]. The presence of ultra nano-sized

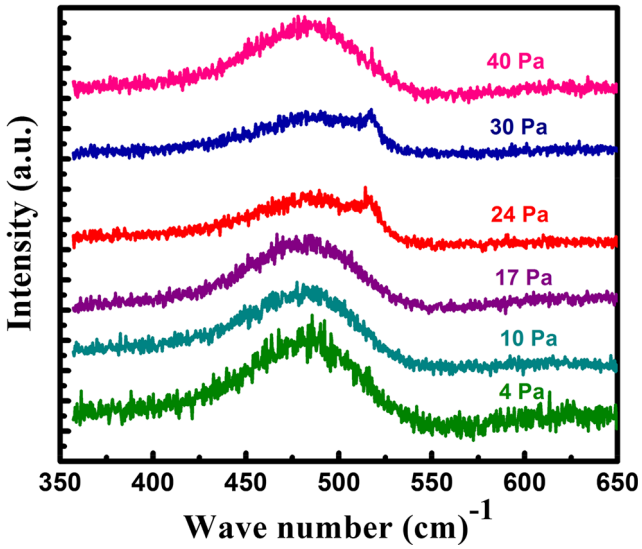

Fig. 4 Raman spectra of silicon films deposited at different pressure

crystallites arises with the appearance of Raman signal at around 490 cm^{-1} (grain boundary phase) which is superimposed on Raman signal of amorphous phases. It was also observed that the characteristic hump observed at 490 cm^{-1} also shifts to peak position at nearly 518 cm^{-1} for film deposited at 24 and 30 Pa respectively. This peak shifting clearly reflects the phase transition from amorphous to crystalline growth. The average crystalline volume fraction in these films is low and the distribution of grains might be non-uniform. For nanocrystalline silicon the Raman peak exhibits a frequency downshift and peak broadening due to phonon confinement effect and stress [57]. From our results, it is clear that at low pressure, films

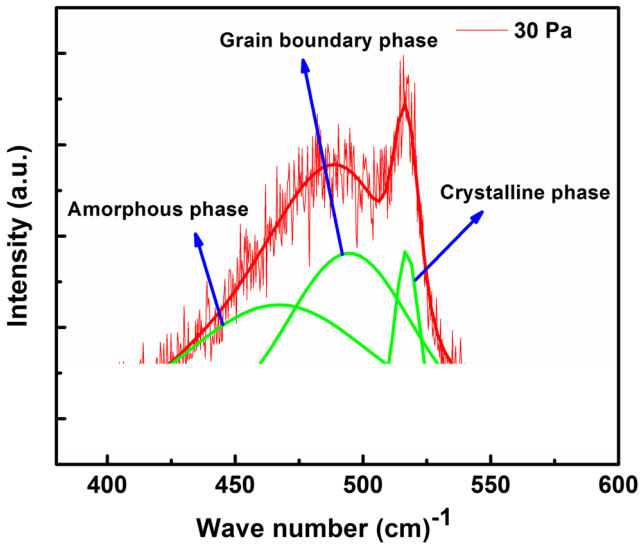

Fig. 5 Decomposition of Raman spectra of film deposited at 30 Pa pressure

are amorphous in nature and ultra nano-sized crystallites are embedded in amorphous silicon matrix that has been identified with broad hump nearly at ~490 cm^{-1} in the Raman spectrum. It is well known that for nano-sized crystallites, the central frequency of the crystalline peak in the spectrum shifts from the bulk crystal value (520 cm^{-1}) to a lower value [58]. The crystallites are extremely nano-sized (<2 nm). Therefore, only small area has been probed so, it is difficult to estimate crystalline volume fraction in these films, also the Raman signal influenced by large number of grain boundaries of these ultra nano-sized crystallites. From Raman analysis, it was observed that films deposited (at 24 and 30 Pa) with lower hydrogen content contain higher crystalline fraction and better silicon (Si-Si) network ordering. The improvement in the structure ordering and increase in crystalline fraction of these films results in stress reduction. From Raman spectroscopy we confirmed with the crystalline growth at pressure 24 and 30 Pa respectively and this might be due to platelet like configuration as observed from the results of IR spectra and resulting in relaxed material within platelets that leads to crystallinity in the structure and crystalline fraction have been quantified using following relation;

$$Xc = \frac{Ic}{Ic + Ia + Ig} \times 10 \tag{4}$$

$$Xa = \frac{Ia}{Ia + Ic + Ig} \times 100 \tag{5}$$

$$Xg = \frac{Ig}{Ig + Ic + Ia} \times 100 \tag{6}$$

Where Ic, Ia, Ig are integrated intensities of crystalline, amorphous and grain boundaries respectively and Xc, Xa, Xg are relative volume fraction of crystalline, amorphous and grain boundary phases respectively [59] and are shown in Table 3.

For nc-Si, the Raman peak can be explained using different theoretical models that compute phonon confinement [60, 61]. For nc-Si, Zi's confinement model using bond polarizability approach with well-defined geometry is used to find average crystallite size for nc-silicon and is given as [62]:

$$\Delta\omega(D) = -A\left(\frac{a}{D}\right)^{\gamma} \tag{7}$$

Where $\Delta\omega\,(D) = (\omega_{c-Si} - \omega_{nc-Si})$, D is crystallite size, a = 0.54 nm; defined as lattice constant of silicon, $\gamma = 1.44$ and A= 47.41 are fixed parameters.

The crystallite size calculated were found to be varying from 2-12 nm which also found to correlate with other morphological observations.

Table 3 Parameters deduced from Raman and AFM analysis

Pressure variation (Pa)	Crystalline fraction (%)	Amorphous fraction (%)	Grain boundary fraction (%)	Maximum roughness (nm)
24	32	30	38	4.82
30	37	26	37	8.52

3.5 X-ray Diffraction

Figure 6 depicts the X-ray diffraction pattern of silicon thin films deposited at different deposition pressures. It is clearly evident from the diffraction pattern, the peaks located around 2θ ~28.4, ~47.3, ~56.1 correspond to <111>, <220> and <311> crystallographic planes of c-Si which demonstrates regular growth of nc-Si:H at process pressure of >17 Pa. These peaks demonstrate the increase in crystalline volume fraction and size of crystallites with increase in deposition pressure up to 30 Pa pressure. The films deposited at lower pressure signify not only the higher contribution of amorphous phase, it can also be related to the smaller size of the crystallites and thus to the higher surface-to-volume ratio. This is supported by crystallite size estimated from Raman spectroscopy and are shown in Table 4. The narrow peak at <111> crystallographic orientation at low process pressure also been observed in the diffraction spectra; this is interpreted due to gradual increase in inclusion of nano-sized crystals in amorphous matrix [63, 64]. The strongest diffraction peak observed at <111> plane in all the samples could be consider to be the preferential growth direction of deposited films. Further, the peak intensity increases with increase in deposition pressure. The increase in intensity of these peaks at pressure >17 Pa confirms relatively large proportion of the platelets formation or hydrogen configurations along c-Si <111> plane which is well correlated with IR spectroscopy and Raman spectroscopy. The characteristic feature of platelets is the fact that the <111> reflection is very strong and all others are weak with a highly ordered pattern as observed in Fig. 6. The average crystalline size was calculated from full width half maxima (FWHM) of peak using the classical Scherrer's formulae:

$$D = \frac{K\lambda}{\beta cos\theta} \tag{8}$$

Where D is average crystallite size, λ is wavelength of Cu-Kα line (1.54A°), K is shape factor equal to 0.94 and β is full width half maxima.

For pressure <24 Pa the crystalline related peaks are not so sharp or grains are not so large enough to be visible clearly. At pressure 30 Pa, the average crystallite size obtained is 18.34 nm. The differences in average crystallite size obtained using Scherrer formulae are due to difference in the FWHM of crystallographic orientations <111>in the deposited films. From results, we observed that the smaller crystalline fraction is not due to higher amorphous fraction, it might be due to increase of void fraction in the films.

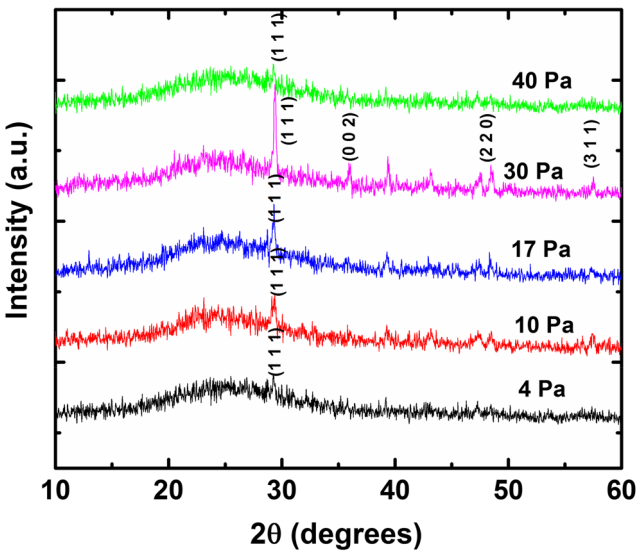

Fig. 6 X-ray diffraction spectra of silicon films at different pressure

3.6 Morphological Observations

Morphological study of deposited films includes both FESEM and AFM techniques. Figure 7 shows the FESEM images. Images evidence the distribution of crystalline grains, amorphous tissues and surrounding grain boundaries. Figure 8 showed the AFM images of deposited silicon thin films at different pressure variation. It is clear from Fig. 8, that the small or bigger crystallites are embedded in amorphous matrix. At pressure 4, 10 and 17 Pa the ultra nano-sized crystallites (<2 nm) are uniformly dispersed in amorphous matrix within the scanned area. With increasing pressure well defined clustering of nano-sized crystallites formation takes place. These morphological observations correlate with other optical and structural results. The film deposited at 24 Pa and 30 Pa shows crystalline fraction 32% and 37% with crystallite size 7 nm and 12 nm as shown in Tables 3, 4 respectively. The reason is that high pressure enhances the contribution of atomic hydrogen in the plasma and provides precursor favourable sites for formation of crystalline phases. The variation of rms roughness estimated from AFM is shown in Table 3.

Table 4 Parameters deduced from optical and electrical studies

Pressure variation (Pa)	Band gap (eV)	Crystallite size (nm)	Dark conductivity $(\Omega\ cm)^{-1}$	Photo conductivity $(\Omega\ cm)^{-1}$	Activation energy (eV)	Deposition rate (A°/s)
4	1.75	2.3	2.84E-9	4.04E-7	0.98	0.85
10	1.78	2.4	1.66E-9	4.91E-6	0.95	0.88
17	1.76	2.7	2.30E-9	1.21E-5	0.87	0.91
24	1.94	7.4	2.00E-9	4.04E-6	0.89	1.03
30	1.89	12.0	1.16E-8	1.84E-5	0.82	1.13
40	1.71	4.0	1.46E-9	3.33E-6	0.75	1.26

3.7 Electronic Properties

Figure 9 shows the temperature dependent conductivity plot of silicon films recorded at different pressure variation. Conductivity was measured from room temperature to 200 °C under vaccum. The values of dark and photoconductivity was calculated using the formulae [6]

$$\sigma = \frac{IL}{VWT} \tag{9}$$

Where 'V' refers to voltage, 'W' is width, 'T' is thickness, 'I' is measured values of current and 'L' is the distance between the electrodes. The illumination intensity of 100 mW/cm^2 was applied from halogen lamp during photoconductivity measurements. There is not much difference in room temperature dark conductivities of all the samples. The conductivity is the measure of average transport of carriers in amorphous and crystalline regions. The electronic or transport property of material basically depends upon the size and volume density of crystallites in the material and heterogeneities. The optical, electrical, structural properties and deposition rate are shown in Table 4. It is clearly observable from results that the films deposited at less than 24 Pa were resulting the dispersion of ultra nano-sized crystallites in amorphous matrix hence there is hardly any variation of size and volume fraction of crystallites with variation of pressure. These films exhibited near to amorphous character, whereas significant crystalline fraction obtained at pressure 24 and 30 Pa, evidencing the abrupt transition. This film also shows higher dark conductivity (1.16 E-8) and photoconductivity (1.84 E-5). It is clearly observed from Fig. 9, the conductivity at 30 Pa is due to crystallinity enhancement in the films. From FTIR spectra, the absorption band

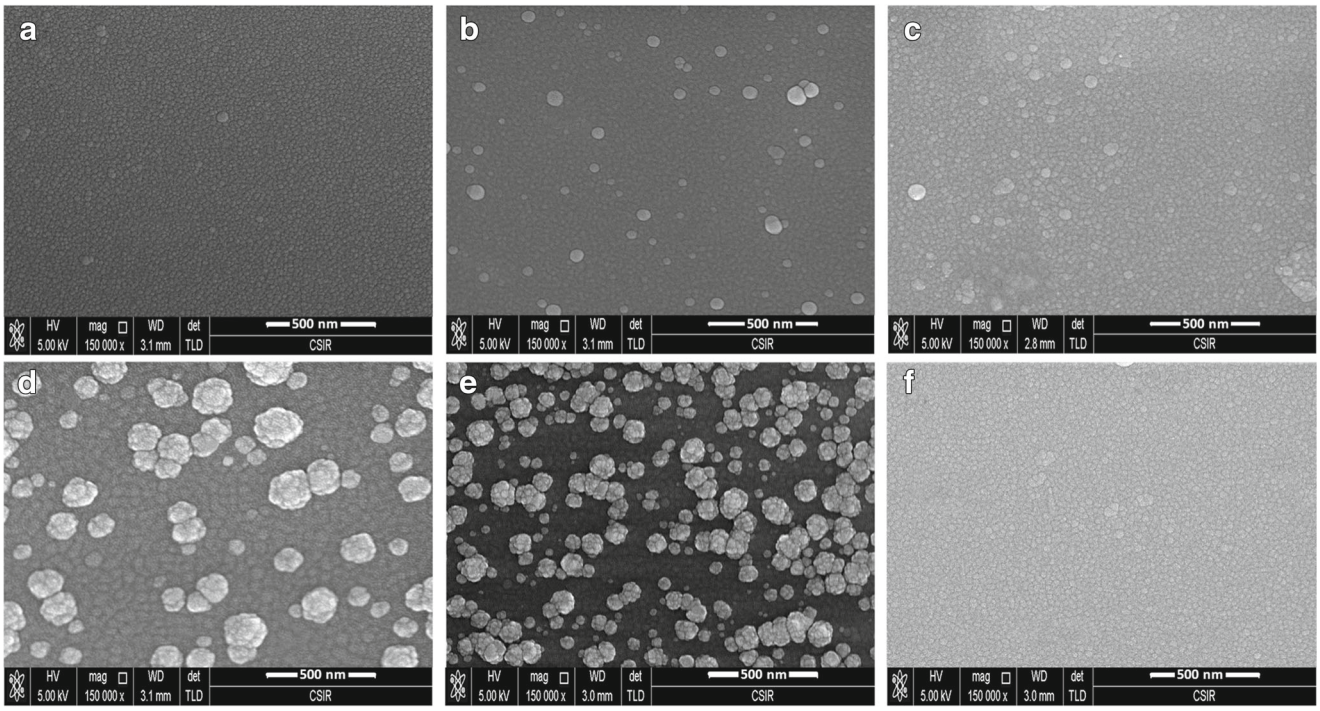

Fig. 7 FESEM images of silicon films deposited at various pressure **a** 4 Pa; **b** 10 Pa; **c** 17Pa; **d** 24 Pa; **e** 30 Pa; **f** 40 Pa

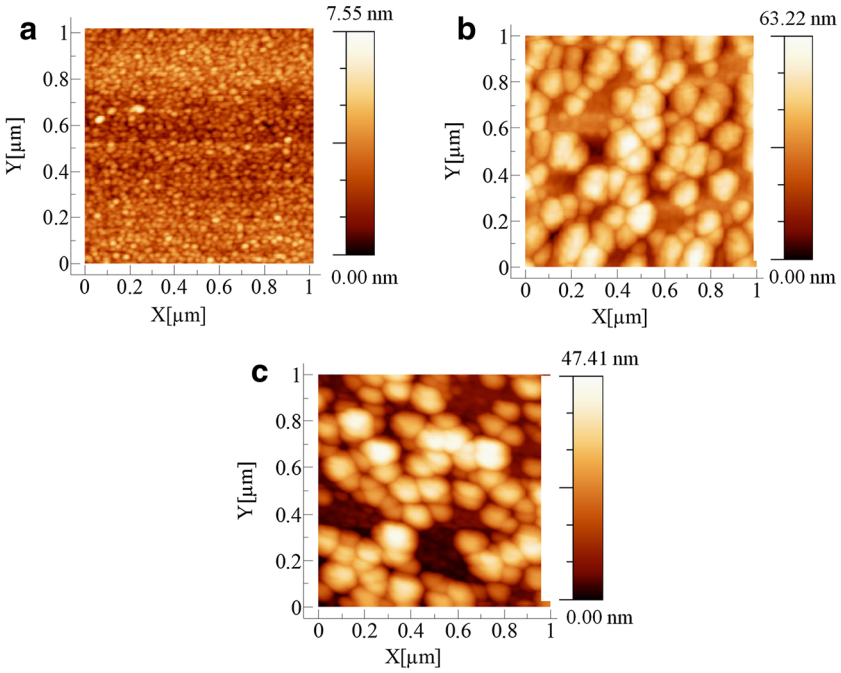

Fig. 8 AFM images of Si:H films as a function of Pressure **a** 17 Pa; **b** 24 Pa; **c** 30 Pa

around 2030 cm^{-1} was observed at pressure 24 and 30 Pa due to presence of hydrogen bonds at internal surface or crystallites. The band gap was also found to be ∼1.9 eV due to transition from amorphous to crystallite phase with variation in crystallite size as obtained from raman measurement. The transitions in the films were observed, as one can see from Figs. 7, 8 respectively. It is also observed that the film deposited at 40 Pa pressure is mainly amorphous in nature beside with the distribution of ultra-nano sized crystallites in silicon matrix. Since secondary gas phase reactions occurs that result in surface etching with increase of pressure. This etches the Si-Si bonds in the network which thus increases the hydrogen content in the deposited film. The deposition rate was found to vary from 0.85 – 1.26 A°/s. The deposition rate varies linearly with pressure. The increase in deposition rate can be understood as a consequence of faster dissociation of precursor gases simultaneously with higher collision possibility at higher pressures. Additionally, the use of high excitation frequency results in higher flux density which might be possible cause for increasing deposition rate over conventional used RF frequency (13.56 MHz). Figure 9 showed the temperature dependent dark conductivity and the plot can be divide into two different regimes due to change in slope at $T = 344$ K. Above this temperature the other regime is linked with thermally activated carriers in a-Si:H which named as extended state conduction (ESC) regime. At lower temperatures T <344 K, there appears to be variable range hopping (VRH) with exponential tail distribution in the gap where electron hop to neighbouring site. From results, transition is seen in transport mechanism from conduction band to extended states to transport phonon assisted hopping in the region of localized states at T = 344 K. The activation energy (Ea) was estimated between 0.75 to 0.98 eV and was shown in Table 4. On the other hand, from Fig. 10, activation energy (Ea) exhibited values of 0.82 eV and 0.89 eV for samples deposited at 24 Pa and 30 Pa respectively. Activation energy was estimated from Arrhenius curve [65]. The temperature dependent conductivity gives some insight related to disorderness in the material i.e. density of defect states in the mid gap region. However, temperature dependent measurements allow the evaluation through extended states only. Dark conductivity exhibits a thermally activated behaviour, whose activation energy helps in

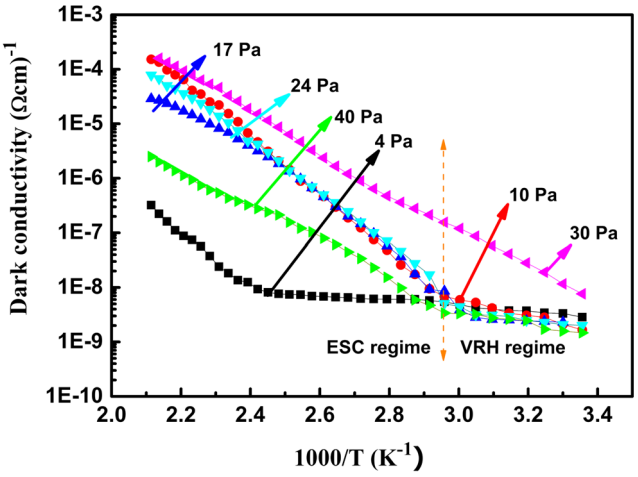

Fig. 9 Temperature dependent conductivity of silicon films at different pressure variation

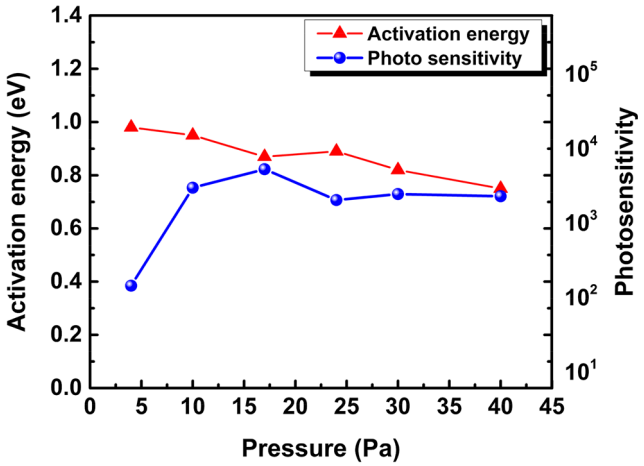

Fig. 10 Activation energy and photosensitivity of silicon films deposited at different pressure

determining the Fermi level position that should be around mid gap. Lower value of dark conductivity indicates the absence of electronically active impurities. However; photoconductivity is expected to reach higher values (1.84 E-5) due to reasonably low recombination of the photo-generated carriers. Photosensitivity is another term defined as ratio of photoconductivity and dark conductivity measured at room temperature. The value of photosensitivity increases might be because of low recombination of photo-generated carriers. Determination of mobility and lifetime of photo-generated carriers gives an additional insight to carrier transport properties which can be investigated separately. It has been reported that [66] the enhanced stability has been associated with the films grown near the transition to nc-Si:H, whose structure supposed to have improved order.

4 Conclusion

The detailed interpretation of IR spectra was used to obtain mutual relation between deposition pressure and different hydrogen bonding configuration in silicon films. The evolution of microstructure at the transition region is related to bonded hydrogen configurations. The isolated Si-H mode and clustered Si-H hydride configuration in voids and vacancies are responsible for the observed structural changes. It has been concluded from results that the films deposited at pressure 24 and 30 Pa, the clustered Si-H mode produces IR peak at nearly 2033 cm^{-1} which might be related to bonded hydrogen in platelet like configuration. Above certain pressure, etching of platelets configuration occurs resulting in internal void formation in the network which is observed at pressure above 30 Pa. So, with pressure variation we suggest that hydrogen platelets configuration in the structure evolves crystallinity and structural changes in silicon thin films. Raman spectroscopy and X-ray diffraction studies clearly shows the transition from amorphous to nanocrystalline growth at 24 and 30 Pa. The films grown in the transition region shows higher dark conductivity, low hydrogen content, wider optical band gap. FESEM and AFM shows the presence of crystallites in the films deposited at pressure <24 Pa.

Acknowledgements The authors are thankful to Director, CSIR-NPL, New Delhi for his kind support and encouragement. We are thankful to silicon thin film group members for their help and support. One of the authors Sucheta Juneja would like to acknowledge science and engineering research board (SERB), govt. of India for providing National Post– Doc Fellowship (NPDF).

References

1. Rech B, Wagner H (1999) Potential of amorphous silicon for solar cells. Appl Phys A 69(2):155–167
2. Juneja S, Sudhakar S, Lodhi K, Sharma M, Kumar S (2014) Kinetics of recovery of light induced defects on thermal annealing towards stability of microcrystalline silicon films. Adv Sci Lett 20(7-8):1499–1503
3. Saleh R, Nickel NH (2003) Raman spectroscopy of B-doped microcrystalline silicon films. Thin Solid Films 427(1):266–269
4. Martins R, Ferreira I, Fortunato E (1995) Wide band gap microcrystalline silicon thin films. In: Solid state phenomena, vol 44. Trans Tech Publications, pp 299–346
5. Yan WS, Wei DY, Guo YN, Xu S, Ong TM, Sern CC (2012) Low-temperature preparation of phosphorus doped μc-Si: H thin films by low-frequency inductively coupled plasma assisted chemical vapor deposition. Thin Solid Films 520(6):1724–1728
6. Juneja S, Sudhakar S, Gope J, Lodhi K, Sharma M, Kumar S (2015) Highly conductive boron doped micro/nanocrystalline silicon thin films deposited by VHF-PECVD for solar cell applications. J Alloys Compd 643:94–99
7. Jadkar SR, Sali JV, Takwale MG, Musale DV, Kshirsagar ST (2001) The role of hydrogen dilution of silane and phosphorus doping on hydrogenated microcrystalline silicon (μc-Si:H) films prepared by hot-wire chemical vapor deposition (HW-CVD) technique. Thin Solid Films 395(1):206–212
8. Ali AM, Kobayashi H, Inokuma T, Al-Hajry A (2013) Morphological, luminescence and structural properties of nanocrystalline silicon thin films. Mater Res Bull 48(3):1027–1033
9. Juneja S, Sudhakar S, Srivastava AK, Kumar S (2016) Morphology and micro-structural studies of distinct silicon thin films deposited using very high frequency plasma enhanced chemical vapor deposition process. Thin Solid Films 619:273–280
10. Smirnov V, Das C, Melle T, Lambertz A, Hülsbeck M, Carius R, Finger F (2009) Improved homogeneity of microcrystalline absorber layer in thin-film silicon tandem solar cells. Mater Sci Eng B 159:44–47
11. Jackson WB, Tsai CC (1992) Hydrogen transport in amorphous silicon. Phys Rev B 45(12):6564
12. Morral AFI, Bertomeu J, Cabarrocas PRI (2000) The role of hydrogen in the formation of microcrystalline silicon. Mater Sci Eng B 69:559–563
13. Guha S (2004) Thin film silicon solar cells grown near the edge of amorphous to microcrystalline transition. Sol Energy 77(6):887–892

14. Shah A, Vallat-Sauvain E, Torres P, Meier J, Kroll U, Hof CH, Droz C, Goerlitzer M, Wyrsch N, Vanecek M (2000) Intrinsic microcrystalline silicon (μc-Si: H) deposited by VHF-GD (very high frequency-glow discharge): a new material for photovoltaics and optoelectronics. Mater Sci Eng B 69:219–226
15. He Y, Yin C, Cheng G, Wang L, Liu X, Hu GY (1994) The structure and properties of nanosize crystalline silicon films. J Appl Phys 75(2):797–803
16. Oliveira EC, Cruz SA, Aguiar PHL (2012) Effect of PECVD deposition parameters on the DLC/PLC composition of aC: H thin films. J Braz Chem Soc 23(9):1657–1662
17. Rath JK, Verkerk AD, Liu Y, Brinza M, Goedheer WJ, Schropp REI (2009) Gas phase considerations for the growth of device quality nanocrystalline silicon at high rate. Mater Sci Eng B 159:38–43
18. Heintze M, Westlake W, Santos PV (1993) Surface controlled plasma deposition and etching of silicon near the chemical equilibrium. J Non-Cryst Solids 164:985–988
19. Cabarrocas PRI, Layadi N, Heitz T, Drevillon B, Solomon I (1995) Substrate selectivity in the formation of microcrystalline silicon: mechanisms and technological consequences. Appl Phys Lett 66(26):3609-3611
20. Shah AV, Meier J, Vallat-Sauvain E, Wyrsch N, Kroll U, Droz C, Graf U (2003) Material and solar cell research in microcrystalline silicon. Sol Energy Mater Sol Cells 78(1):469–491
21. Kondo M, Matsuda A (2004) Novel aspects in thin film silicon solar cells–amorphous, microcrystalline and nanocrystalline silicon. Thin Solid Films 457(1):97–102
22. Bhattacharya K, Das D (2007) Nanocrystalline silicon films prepared from silane plasma in RF-PECVD, using helium dilution without hydrogen: structural and optical characterization. Nanotechnology 18(41):415704
23. Tauc J (2012) Amorphous and liquid semiconductors. Springer, Berlin
24. Jadhavar A, Pawbake AM, Waykar R, Jadkar V, Kulkarni R, Bhorde A, Rondiya S et al (2017) Growth of hydrogenated nanocrystalline silicon (nc-Si: H) films by plasma enhanced chemical vapor deposition (PE-CVD). Energy Procedia 110:45–52
25. Kumar S, Dixit PN, Rauthan CMS, Parashar A, Gope J (2008) Effect of power on the growth of nanocrystalline silicon films. J Phys Condens Matter 20(33):335215
26. Mullerova J, Jurecka S, Sutta P (2006) Optical characterization of polysilicon thin films for solar applications. Sol Energy 80(6):667–674
27. Wang Y, Lin J, Huan CHA (2003) Structural and optical properties of a-Si: H/nc-Si: H thin films grown from Ar–H_2–SiH_4 mixture by plasma-enhanced chemical vapor deposition. Mater Sci Eng B 104(1):80–87
28. Vasiliev I, Öğüt S, Chelikowsky JR (2001) Ab initio absorption spectra and optical gaps in nanocrystalline silicon. Phys Rev Lett 86(9):1813
29. Sun C, Chen TP, Tay BK, Li S, Zhang YB, Huang H, Pan LK, Lau SP, Sun XW (2001) An extended quantum confinement' theory: surface-coordination imperfection modifies the entire band structure of a nanosolid. J Phys D Appl Phys 34(24):3470
30. Fischer M, Tan H, Melskens J, Vasudevan R, Zeman M, Smets AHM (2015) High pressure processing of hydrogenated amorphous silicon solar cells: relation between nanostructure and high open-circuit voltage. Appl Phys Lett 106(4):043905
31. Kroll U, Meier J, Mikhailov ASS, Weber J (1996) Hydrogen in amorphous and microcrystalline silicon films prepared by hydrogen dilution. J Appl Phys 80(9):4971–4975
32. Finger F, Carius R, Dylla T, Klein S, Okur S, Gunes M (2003) Stability of microcrystalline silicon for thin film solar cell applications. IEE Proceedings-Circuits, Devices and Systems 150:300–308
33. Matsui T, Matsuda A, Kondo M (2006) High-rate microcrystalline silicon deposition for p–i–n junction solar cells. Sol Energy Mater Sol Cells 90(18):3199–3204
34. Green ML, Gusev EP, Degraeve R, Garfunkel EL (2001) Ultrathin (4 nm) SiO_2 and Si–O–N gate dielectric layers for silicon microelectronics: understanding the processing, structure, and physical and electrical limits. J Appl Phys 90(5):2057–2121
35. Shah AV, Meier J, Vallat-Sauvain E, Wyrsch N, Kroll U, Droz C, Graf U (2003) Material and solar cell research in microcrystalline silicon. Sol Energy Mater Sol Cells 78(1):469–491
36. Plaza-Castillo J, García-barrientos A, Moreno-Moreno M, Arellano-Jiménez MJ, Vizcaíno KY, Bernal JL (2016) Analysis of H_2 and SiH_4 in the deposition of pm-Si: H thin films by pecvd process for solar cell applications. Microsc Microanal 22(S3):1874–1875
37. Juneja S, Verma P, Savelyev DA, Khonina SN, Sudhakar S, Kumar S (2016) Effect of power on growth of nanocrystalline silicon films deposited by VHF PECVD technique for solar cell applications. AIP Conf Proc 1724:020016
38. Langford AA, Fleet ML, Nelson BP, Lanford WA, Maley N (1992) Infrared absorption strength and hydrogen content of hydrogenated amorphous silicon. Phys Rev B 45(23):13367
39. Smets AHM, van de Sanden MCM (2007) Relation of the Si- H stretching frequency to the nanostructural Si-H bulk environment. Phys Rev B 76(7):073202
40. Vignoli S, Morral AFI, Butté R, Meaudre R, Meaudre M (2002) Hydrogen related bonding structure in hydrogenated polymorphous and microcrystalline silicon. J Non-Cryst Solids 299:220–225
41. Gleason KK, Petrich MA, Reimer JA (1987) Hydrogen microstructure in amorphous hydrogenated silicon. Phys Rev B 36(6):3259
42. Zhang SB, Jackson WB (1991) Formation of extended hydrogen complexes in silicon. Phys Rev B 43(14):12142
43. Johnson NM, Doland C, Ponce F, Walker J, Anderson G (1991) Hydrogen in crystalline semiconductors: a review of experimental results. Phys B Condens Matter 170(1):3–20
44. Jackson WB, Tsai CC (1992) Hydrogen transport in amorphous silicon. Phys Rev B 45(12):6564
45. Marra DC, Edelberg EA, Naone RL, Aydil ES (1998) Silicon hydride composition of plasma-deposited hydrogenated amorphous and nanocrystalline silicon films and surfaces. J Vac Sci Technol A 16(6):3199–3210
46. Keudell AV, Abelson JR (1998) The interaction of atomic hydrogen with very thin amorphous hydrogenated silicon films analyzed using in situ real time infrared spectroscopy: reaction rates and the formation of hydrogen platelets. J of Appl Phys 84(1):489–495
47. Agarwal S, Hoex B, van de Sanden MCM, Maroudas D, Aydil ES (2004) Hydrogen in Si-Si bond center and platelet-like defect configurations in amorphous hydrogenated silicon. J Vac Sci Technol B 22(6):2719–2726
48. Niwano M, Kageyama J, Kurita K, Kinashi K, Takahashi I, Miyamoto N (1994) Infrared spectroscopy study of initial stages of oxidation of hydrogen-terminated Si surfaces stored in air. J Appl Phys 76(4):2157–2163
49. Juneja S, Sudhakar S, Khonina SN, Skidanov RV, Porfirevb AP, Moissev OY, Kazanskiy NL, Kumar S (2016) Nanocrystalline silicon thin films and grating structures for solar cells. In: Optical technologies for telecommunications 2015, vol 9807. International Society for Optics and Photonics, p 98070F

50. Kondo M, Matsuda A (2002) An approach to device grade amorphous and microcrystalline silicon thin films fabricated at higher deposition rates. Curr Opin Solid State Mater Sci 6(5):445–453
51. Xu L, Li ZP, Wen C, Shen WZ (2011) Bonded hydrogen in nanocrystalline silicon photovoltaic materials: impact on structure and defect density. J Appl Phys 110(6):064315
52. Vignoli S, Butte R, Meaudre R, Meaudre M, Brenier R (2003) Links between hydrogen bonding, residual stress. structural properties and metastability in hydrogenated nanostructured silicon thin films. J Phys Condens Matter 15(43):7185
53. Van Veen MK, Van der Werf CHM, Rath JK, Schropp REI (2003) Incorporation of amorphous and microcrystalline silicon in n–i–p solar cells. Thin Solid Films 430(1):216–219
54. Street RA (1991) Hydrogen chemical potential and structure of a-Si: H. Phys Rev B 43(3):2454
55. Tsu DV, Chao BS, Ovshinsky SR, Jones SJ, Yang J, Guha S, Tsu R (2001) Heterogeneity in hydrogenated silicon: evidence for intermediately ordered chainlike objects. Phys Rev B 63(12):125338
56. Gope J, Kumar S, Singh S, Rauthan CMS, Srivastava PC (2012) Growth of mixed-phase amorphous and ultra nanocrystalline silicon thin films in the low pressure regime by a VHF PECVD process. Silicon 4(2(2012)):127–135
57. Richter H, Wang ZP, Ley L (1981) The one phonon raman spectrum in microcrystalline silicon. Solid State Commun 39(5):625–629
58. Juneja S, Sudhakar S, Gope J, Kumar S (2015) Mixed phase silicon thin films grown at high rate using 60 MHz assisted VHF-PECVD technique. Mater Sci Semicond Process 40:11–19
59. Trung TQ, Jiri S, Stuchlikova H, Dinh NN, Khuong HK, Quynh PTN, Nga NTH (2009) The effects of hydrogen dilution on structure of Si: H thin films deposited by PECVD. J Phys Conf Series 187(1):012035
60. Campbell IH, Fauchet PM (1986) The effects of microcrystal size and shape on the one phonon raman spectra of crystalline semiconductors. Solid State Commun 58(10):739–741
61. Fauchet PM, Campbell IH (1988) Raman spectroscopy of low-dimensional semiconductors. Crit Rev Solid State Mater Sci 14(S1):s79–s101
62. Zi J, Buscher H, Falter C, Ludwing W, Zhang K, Xie X (1996) Raman shifts in Si nanocrystals. Appl Phys Lett 69(2):200–202
63. Agarwal S, Hoex B, van de Sanden MCM, Maroudas D, Aydil ES (2004) Hydrogen in Si–Si bond center and platelet-like defect configurations in amorphous hydrogenated silicon. J Vac Sci Technol, B: Microelectron Nanometer Struct–Process, Meas, Phenom 22(6):2719–2726
64. Samanta S, Das D (2018) Microstructural association of diverse chemical constituents in nc-SiO x: H network synthesized by spontaneous low temperature plasma processing. Physica E: Low-dimensional Systems and Nanostructures
65. Chaudhary D, Sharma M, Sudhakar S, Kumar S (2018) Effect of pressure on bonding environment and carrier transport of a-Si: H thin films deposited using 27.12 MHz Assisted PECVD process. Silicon 10(1):91–97
66. Ray S, Mukhopadhyay S, Jana T (2006) Studies on microstructure of silicon thin films and its effect on solar cells. Sol Energy Mater Sol Cells 90(5):631–639